CHAPTER 4

Sliding Bifurcations in a dry friction oscillator

"Une cause trés petite qui nous échape détermine un effect considérable
que nous ne pouvons pas ne pas voir,
et alors nous disons que cet effet est du au hasard."

J.H.Poincaré (1854-1912)

In this chapter a dry friction oscillator is investigated. This system is affected by discontinuity-induced bifurcations (DIBs) due to "stick-slip" motions. Such bifurcations have been recently classified as *sliding bifurcations* and are a characteristic feature of so-called Filippov systems. Basically, four distinct cases of such bifurcations can be identified: *crossing-sliding*, *grazing-sliding*, *switching-sliding* and *adding-sliding*. We present detailed examples of all these different bifurcation scenarios. Furthermore, a degenerate switching-sliding bifurcation is shown. In that case of degenerate switching-sliding bifurcation two curves of codimension-one sliding bifurcation, crossing-sliding and adding-sliding, branch out from the codimension-two point. Also, a smooth codimension-two cusp bifurcation is presented. Coexistence of periodic orbits in the region between both fold codimension-one curves is shown to exist by means of domain of attraction diagrams using a cell-to-cell mapping method.

4.1 Introduction

Dry friction is a very common phenomenon in nature and in many mechanical systems such as bearings, transmissions, hydraulic and pneumatic cylinders, valves, gratings brakes and wheels... It appears at the physical interface between two surfaces in contact and is the source of self-sustained oscillations, also known as stick-slip vibrations. Furthermore, friction constitutes an important aspect of many other disciplines such as seismology and tectonic fault dynamics [26, 32, 85, 113], acoustics [102, 127] and more.

Systems with friction have been studied extensively by researchers since the historical works of Amontons [5] and Coulomb [37] but not been fully understood yet. Indeed, new friction models are continuously being presented [4]. However, only in the last 10-15 years, these systems and their bifurcations have been investigated as nonsmooth dynamical systems.

A simple single-degree-of-freedom nonsmooth oscillator under self and/or external-excitation is commonly used to describe the behaviour of stick-slip systems. In [124] it is shown that beside the well-know periodic limit cycle, chaotic motion is also possible in oscillators with external forcing. A rich bifurcational behaviour (period-doubling, intermittency) under parameter variations is exhibited. In further investigations [83, 125] such bifurcational behaviour predicted by numerical simulations is compared with experimental results showing a good agreement. In others works a damper is also included in the model. For this type of system non-standard bifurcations such as discontinuous fold bifurcations are detected in [73, 98].

Several works consider the problem of bifurcations and chaos in a two block stick-slip system as [70, 72, 73, 75, 103]. A one-dimensional discontinuous map termed as *event-map* is introduced in order to explain discontinuity-induced bifurcations (DIBs). In [10] a smoothing procedure is applied to illustrate different bifurcational behaviours such as period-doubling route to stick-slip chaos, stick-slip hyper-chaos and quasi-periodic attractors.

Stick-slip systems are important examples of Filippov systems (systems with discontinuous vector fields). The stick phase in these systems can be considered as a motion constrained to some subset of the state space. Then, such constrained motion can be linked with the so-called *sliding mode* studied in [64, 143, 144]. Thus, periodic stick-slip motion in friction oscillators corresponds to periodic orbits characterised by segments of sliding modes, or *sliding orbits* as they were recently termed in the literature.

Nonsmooth dynamical systems can undergo not only standard bifurcations (such as fold, flip and Hopf bifurcations) but also can exhibit an en-

tirely novel class of bifurcations that cannot be explained in terms of classical bifurcation theory for smooth systems. These are often termed as *DIBs* (also referred to as nonsmooth bifurcations or C-bifurcations) to distinguish them from the bifurcations also occurring in smooth systems. In particular, Filippov systems can exhibit four generic types of codimension-one DIBs of limit cycles termed as *sliding bifurcations*, namely, the *crossing-sliding*, *grazing-sliding*, *switching-sliding* and *adding-sliding* bifurcations [51, 95]. Only the grazing-sliding bifurcation scenario might cause an abrupt transition to different attractors under small variation of the bifurcation parameter. For instance, in [52] it is shown that the sudden onset of chaotic stick-slip oscillations observed in [149] is due to the grazing-sliding scenario. In the others scenarios stability properties and period of the cycles remain unchanged.

Several examples have illustrated each case of sliding bifurcation. For instance, in [51] a third-order relay system is used as numerical example. In [91] a example of a friction oscillator with Coulomb friction consisting of a static friction coefficient equal to the kinetic friction coefficient is considered, while a modified Coulomb friction with a cubic nonlinearity, firstly introduced by Yoshitake and Sueoka in [149], is the subject of study in [52]. In this paper an approximation to a measured friction characteristic introduced by [125] will be considered to investigate each type of sliding bifurcation.

Most of the analysis of DIBs has focused so far on the transitions that can be observed under variation of one of the system parameter. Although a classification of smooth codimension-two bifurcations is completely established, see [77, 96, 147], only recent works have been addressed to the classification of nonsmooth codimension-two bifurcations. In [92] a first attempt of classification is suggested. A codimension-two DIB can be put into one of three general types: (a) degenerate limit cycles, (b) non-hyperbolic critical cycles or (c) simultaneous occurrence of two grazings. Degenerate sliding bifurcations that belong to the first general type are discussed in [91] and a degenerate crossing-sliding bifurcation is shown in a dry-friction oscillator with Coulomb friction. Bifurcations belonging to the second class have been illustrated in the mentioned dry-friction oscillator introduced by Yoshitake and Sueoka. A flip-grazing and a fold-grazing bifurcation is shown in [92] and [110] respectively.

This chapter will deal with sliding bifurcations of codimension-one and two in an external-excited dry-friction oscillator. An event-driven method to simulate Filippov systems is used to illustrate such bifurcations. Also,

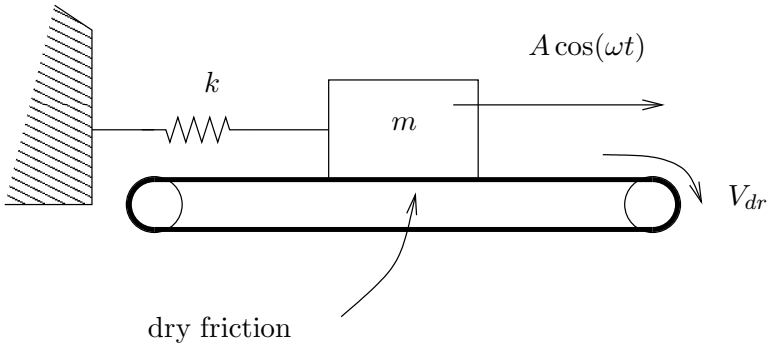

Figure 4.1: Block subject to a spring force, a friction force with a moving belt and an harmonic force of angular frequency ω.

a smoothed version based on the use of an arctan function is considered in order to compare both numerical techniques. A cell mapping method serves to study coexistence of solutions in the region between two fold codimension-one curves merging in a smooth cusp codimension-two bifurcation.

The chapter is organized as follows. Section 4.2 introduces the mechanical model that we use in this paper and discusses the friction force. Section 4.3 is a brief introduction to Filippov systems and sliding motion, while Section 4.5 gives an overview of the algorithms available to simulate Filippov systems. In Section 4.6 we present the numerical simulations for our system and study the bifurcation diagrams for both the discontinuous and smoothed versions of the friction force. Section 4.7 is devoted to show the existence of a degenerate switching-sliding bifurcation. In Section 4.8 a smooth cusp codimension-two is shown and coexistence of periodic orbits in the region between both fold codimension-one curves is manifested by means of domain of attraction diagrams using a cell-to-cell mapping method. Finally, we summarize our conclusions in Section 4.9.

4.2 Description of the model

The nonsmooth system to be investigated, shown in Figure 4.1, is composed of a block of mass m on a belt which moves with constant velocity V_{dr}. The block is connected to a fixed support by a linear spring of stiffness k and is under the action of a sinusoidal external force of magnitude A and frequency ω. The origin of the displacement of the block y is taken where

the spring is unstretched. The block can either ride on the belt, with zero relative velocity with respect to it, or slip on it. In the first case, called the *stick phase*, the motion of the block is uniform and obeys the following algebraic equation

$$y(t) = y(t_0) + V_{dr}(t - t_0), \tag{4.1}$$

The static friction force $F_{fr,s}$ is then in equilibrium with the other forces acting on the block, so that

$$-\mu_s mg < F_{fr,s} = ky - A\cos(\omega t) < \mu_s mg. \tag{4.2}$$

In the second case, referred to as *slip phase*, the motion is governed by the following ordinary differential equation:

$$m\ddot{y} + ky = A\cos(\omega t) + F_{fr,k},\ F_{fr,k} = \mu(v_{rel})mg \tag{4.3}$$

The transition between the stick motion of equation (1) and the slip motion of equation (3) occurs when the static friction force required for equilibrium in equation (2) overcomes either of its threshold values $\pm\mu_s mg$, where μ_s is the static friction coefficient and mg is the weight of the block. When such a transition occurs an accelerated motion begins for the block. The dynamic behavior of the system will be determined by the choice of the model for the *kinetic* friction force $F_{fr,k}(v_{rel})$, where $v_{rel} = V_{dr} - \dot{y}$ is the relative velocity. The kinetic force may assume different forms, being the Coulomb friction one of the most common. The expression is given by a constant friction coefficient μ_0 smaller than the static friction coefficient μ_s:

$$\mu_I(v_{rel}) = \begin{cases} \mu_0 & if \quad v_{rel} > 0 \\ -\mu_0 & if \quad v_{rel} < 0 \end{cases} \tag{4.4}$$

Because of the jump in the characteristic, the transition from stick to slip is not continuous. A different version of Coulomb friction is given by:

$$\mu_{II}(v_{rel}) = \begin{cases} \dfrac{\alpha}{1 + \gamma\,|v_{rel}|} + \beta + \eta \cdot v_{rel}^2 & if \quad v_{rel} > 0 \\ \dfrac{-\alpha}{1 + \gamma\,|v_{rel}|} - \beta - \eta \cdot v_{rel}^2 & if \quad v_{rel} < 0 \end{cases} \tag{4.5}$$

This kinetic friction is an approximation to a measured friction characteristic [125]. Here, the transition from static to kinetic friction is continuous but not differentiable. In the present chapter this later friction characteristic will be adopted.

In the simulations presented below some of the parameters are kept fixed, namely $m = 1$, $k = 1$, $g = 10$, $V_{dr} = 1$, $\alpha = 0.3$, $\gamma = 1.42$, $\beta = 0.1$, $\eta = 0.01$, whereas A and ω will be varied.

4.3 Filippov systems

As mentioned in the Introduction, the dry friction oscillator considered is an example of systems with a discontinuous vector field, the so called Filippov systems. What characterizes such a system is the division of the state space into disjoint subregions, such that in each region the defining vector field is smooth. The boundaries between the different regions will be referred to as *discontinuity* surfaces. In this section only a brief introduction to Filippov systems will be given, and for a more thorough exposition of this topic the reader is referred to [51, 64, 98, 95].

We consider a sufficiently small region $D \in \mathbb{R}^n$ of phase space. To simplify, let us assume that the state space consists of only two subspaces, S_1 and S_2, separated by a discontinuous surface Σ, which is defined by a smooth scalar function $h(x)$ such that

$$\Sigma = \{x \in \mathbb{R}^n : h(x) = 0\}, \tag{4.6}$$

and where

$$S_1 = \{x \in \mathbb{R}^n : h(x) > 0\}, \text{ and } S_2 = \{x \in \mathbb{R}^n : h(x) < 0\}, \tag{4.7}$$

Hence, the equations governing the system flow can be written as

$$\dot{x} = \begin{cases} F_1(x, \mu) & \text{for } S_1, \\ F_2(x, \mu) & \text{for } S_2, \end{cases} \tag{4.8}$$

where F_1, F_2 are sufficiently smooth vector functions and $\mu \in R^m$ is the vector of system parameters.

If the vector fields F_1 and F_2 are locally both pointing away from or towards the discontinuity surface Σ, as depicted in Fig. 4.2 the dynamics is assumed to be locally constrained to the surface until reaching some point on it where one of the two vector fields, F_1 or F_2, changes its direction. The solution which lies within the discontinuity surface is termed as a sliding motion (as mentioned in 4.1, for mechanical systems with friction the term "sticking" is used). The open subset $\hat{\Sigma}$ of the surface Σ where the vector fields are both pointing towards or away from Σ is often referred to as the *sliding surface*. If it holds that

$$\langle \nabla h, F_1 \rangle - \langle \nabla h, F_2 \rangle < 0 \tag{4.9}$$

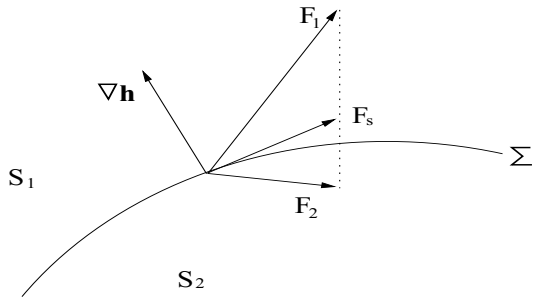

Figure 4.2: Stable sliding mode

then $\hat{\Sigma}$ is stable, while if

$$\langle \nabla h, F_1 \rangle - \langle \nabla h, F_2 \rangle > 0 \tag{4.10}$$

the sliding surface is unstable. Here ∇h denotes a vector which is normal to Σ and $\langle \nabla h, F_i \rangle$ denotes the component of the vector field F_i along the normal to Σ.

Using Utkin's equivalent control method [143, 144] the dynamical system (4.8) can be extended to include the vector field F_s on the sliding surface. We can derive the vector field F_s as a vector function belonging to the convex hull of F_1 and F_2

$$F_s(x) = \frac{F_1(x) + F_2(x)}{2} + \frac{F_2(x) - F_1(x)}{2} s(x), \tag{4.11}$$

where $-1 \leq s(x) \leq 1$. Since the motion is constrained to the sliding surface $\hat{\Sigma}$, F_s must be tangent to Σ, i.e. $\langle \nabla h, F_s \rangle = 0$, which yields

$$s(x) = -\frac{\langle \nabla h, F_1 \rangle + \langle \nabla h, F_2 \rangle}{\langle \nabla h, F_2 \rangle - \langle \nabla h, F_1 \rangle}. \tag{4.12}$$

We can now define the sliding region as

$$\hat{\Sigma} = \{x \in \Sigma : |s(x)| < 1\}, \tag{4.13}$$

with boundaries

$$\partial\Sigma = \{x \in \Sigma : |s(x)| = 1\}, \tag{4.14}$$

$$\partial\Sigma^+ = \{x \in \Sigma : s(x) = 1\}, \tag{4.15}$$

$$\partial\Sigma^- = \{x \in \Sigma : s(x) = -1\}. \tag{4.16}$$

The general setting presented above takes the following particular form for the system under investigation:

$$x = \{y, \dot{y}\}^T \in \mathbb{R}^2, \tag{4.17}$$

$$\Sigma = \{x \in \mathbb{R}^2 : h(x) = \dot{y} - V_{dr} = 0\}, \tag{4.18}$$

$$S_1 = \{x \in \mathbb{R}^2 : h(x) = \dot{y} - V_{dr} < 0\}, \text{ and } S_2 = \{x \in \mathbb{R}^2 : h(x) = \dot{y} - V_{dr} > 0\}, \tag{4.19}$$

$$\dot{x} = \left\{ \begin{array}{c} \dot{y} \\ \ddot{y} \end{array} \right\} = F_1(x, \omega) = \left\{ \begin{array}{l} \dot{y}, \\ -y + A\cos(\omega t) + F_{fr,k} \quad \text{for } S_1, \end{array} \right. \tag{4.20}$$

$$\dot{x} = \left\{ \begin{array}{c} \dot{y} \\ \ddot{y} \end{array} \right\} = F_2(x, \omega) = \left\{ \begin{array}{l} \dot{y}, \\ -y + A\cos(\omega t) - F_{fr,k} \quad \text{for } S_2, \end{array} \right. \tag{4.21}$$

$$\nabla h = (0, 1)^T, \tag{4.22}$$

$$\hat{\Sigma} = \{x \in \Sigma : |(-y + A\cos(\omega t))/F_{fr,s}| < 1\}. \tag{4.23}$$

From a bifurcation point of view, *sliding bifurcations* are characteristic features of Filippov systems. In [51, 52] sliding bifurcations are defined as bifurcations due to interactions between a periodic orbit and the boundary of the sliding region. Following this definition we can distinguish the four possible bifurcations scenarios involving sliding: crossing-sliding, grazing-sliding, switching-sliding and adding-sliding (see section 4.4).

4.4 Sliding Bifurcations: an overview

References [51, 52] define sliding bifurcations as bifurcations due to interactions between a periodic orbit and the boundary of the sliding region. Following this definition we can distinguish four possible bifurcations scenarios involving sliding (see Fig. 4.3). We will present a briefly description and the analytical conditions that must hold for each case.

4.4.1 Crossing-sliding

Figure 4.3 depicts the scenario that is termed as crossing-sliding. Under parameter variation the trajectory, initially composed of three branches, one in the subspace S_1, one in the sliding region and one in the subspace where S_2, intersects the boundary of the sliding region and then switches from a subspace to the other with no sliding portion. For this scenario

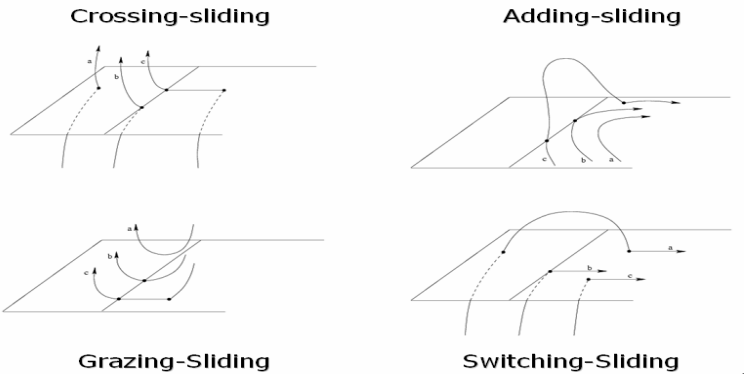

Figure 4.3: Four possible scenarios of sliding bifurcations.

we can associate the following analytical conditions describing the system properties at the bifurcation point:

$$h(x^*) = 0, \nabla h(x^*) \neq 0, \tag{4.24}$$

$$\langle \nabla h, F_1 \rangle (x^*) = 0, \tag{4.25}$$

$$\langle \nabla h, \frac{\partial F_1}{\partial x} F_1 \rangle (x^*) > 0. \tag{4.26}$$

4.4.2 Grazing-sliding

A different bifurcation event, which is called switching-sliding, is depicted in Fig. 4.3. In the case presented in Fig. 4.3, instead, a section of trajectory lying in one region grazes the boundary of the sliding region. This causes the formation of a section of sliding motion. This bifurcation is termed as grazing-sliding. This kind of bifurcation may cause a sudden jump to chaos (see [52] for further details).

In this case the same analytical conditions (4.24), (4.25) and (4.26) given to describe crossing-sliding bifurcations do supply.

4.4.3 Switching-sliding

Under parameter variation the trajectory, initially completely contained in the subspace S_1 and in the sliding region, intersects its boundary and then passes from the subspace S_1 to the other, S_2, and from this to the sliding region.

Conditions (4.24) and (4.25) hold for this case as well, since at the bifurcation point $F_s = F_1$. Moreover, we require an extra condition given by

$$\langle \nabla h, \frac{\partial F_1}{\partial x} F_1 \rangle (x^*) < 0. \tag{4.27}$$

4.4.4 Adding-sliding

The fourth and last case is the so-called adding-sliding, shown also in Fig. 4.3. It differs from the scenarios presented above because the segment of the trajectory that undergoes the bifurcation lies entirely within the sliding region. As a parameter is varied a sliding portion of the trajectory hits tangentially the boundary of the sliding region. Further variation of the parameter causes the formation of a additional segment of trajectory above (or below) the sliding region.

In the case of adding-sliding, conditions (4.24) and (4.25) are still valid but are not sufficient to describe the tangency of the sliding flow to the boundary of the sliding region typical of this scenario. Instead, the following additional condition must also hold:

$$\langle \nabla h, \frac{\partial F_1}{\partial x} F_1 \rangle (x^*) = 0. \tag{4.28}$$

Moreover, in this case the sliding flow has a local minimum with respect to the boundary $\partial\Sigma^-$. Thus, we have

$$\langle \nabla h, (\frac{\partial F_1}{\partial x})^2 F_1 \rangle (x^*) < 0. \tag{4.29}$$

4.5 Numerical simulations methods

If the friction characteristic follows a Coulomb's friction law it is possible to find explicit expressions for the solutions of (4.20) and (4.21). However, considering the friction law given by (4.5) a different numerical treatment for simulation is needed because no analytical solution is available. Basically, simulation techniques for nonsmooth dynamical systems can be classified into three different approaches: event-driven methods, time-stepping methods and smoothing methods.

Event-driven methods are based on the location of any nonsmooth events as accurately as possible. This idea can be compared with the idea for simulating nonsmooth systems with a time-stepping method, which is to recast the nonsmoothness in terms of a complementarity formulation.

Then, one can use time stepping methods accompanied with nonsmooth problem (NSP) solvers to simulate the systems without the need for accurate event detection. That is, the solver can only note that one or more events have occured during a time step without finding the actual event time and location. Such methods have been proven to be effective in simulating mechanical systems with a large number of constraints. However, they suffer from the disadvantage that they are typically only low-order algorithms and some nonsmooth events can be lost. Another strategy to simulate nonsmooth systems, that has been followed in different papers, is to approximate the nonsmooth system with a smooth one. Then, the dynamics of the resulting approximate system is governed by differential equations with sufficient smoothness to be handled through standard numerical techniques. However, a drawback of this method is that an accurate simulation requires the use of very stiff approximate laws. Therefore, the result is a time consuming simulation because the time-stepping procedures have to resort to a very small step-length. Moreover, the effect of the artificial modifications may blur the simulation results.

In [123] an event-driven method to simulate Filippov systems with accurate computing of sliding motions is implemented in a general way in MatLab. We will use this event-driven method in order to perform simulations for our system. The choice of a suitable method to integrate the smooth ODE system to a desired tolerance (within certain limitations) is then required. We have used the fourth-order Runge-Kutta solver that is frequently used for dissipative systems. The routines to locate the surface crossings are the ones built in MatLab. We will also use a smoothing method in order to compare with the event-driven method. The nonsmooth law (4.5) will be uniformly recovered with the following smoothed version

$$\mu_{III}(v_{rel}) = \frac{2}{\pi}\arctan(c_1 v_{rel})\mu_{II}(v_{rel}). \tag{4.30}$$

The parameter $c_1 > 0$ controls the shape of the smooth approximation. In Fig. 4.4 the friction law (4.30) is used with several values of c_1. It is seen that, for c_1 large enough, (4.30) describes almost exactly the properties of the function (4.5). In this paper we will use stiff integration methods built in MatLab, such as `ode23tb` and `ode23s`, to simulate our system with this smooth friction law and $c_1 = 10^8$ in order to obtain accurate results.

We are also interested in the understanding of qualitative changes in the dynamical behaviour by variation of the parameters A and ω. Therefore, numerical simulation techniques for stability and bifurcation analysis will be used.

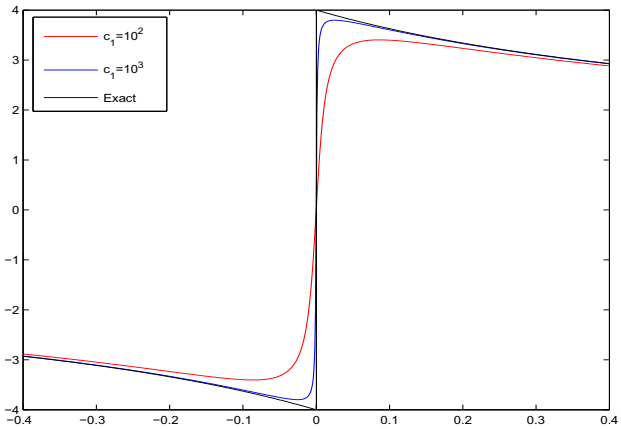

Figure 4.4: Influence of c_1 for the friction approximation given by (4.30).

In order to study the stability of our system we will use a discontinuous one-dimensional map P_{trans} derived from the numerical computation of the exact states of transition from the stick mode to the slip mode (see [125] for further details and [70] for a similar application). This map gives stable solutions but also the unstable solutions of any periodicity and can be defined by

$$\begin{aligned} P_{trans}: \ [0,2\pi] &\rightarrow [0,2\pi] \\ P_{trans}: \phi = \omega t_0 &\rightarrow \phi' = \omega t_1 \end{aligned}$$

where ϕ is the phase angle at a stick-slip transition and ϕ' is the phase angle at the next stick-slip transition. Intersection points of the map P_{trans} with the bisection line $D = \{(x,x)|x \in \mathbb{R}\}$ indicate period-one orbits corresponding to the equation $P_{trans}(\phi) = \phi$. In addition, intersection points of the bisection line D with the graph P^k_{trans} indicate k-periodic orbits. Then, the stability of periodic solutions can be evaluated by the slope of the map P^k_{trans} in the intersection point.

In contrast to the nonsmooth characteristic (4.5), for the smoothed version (4.30) a stick mode does not exist, and a different approach for the map P_{trans} is needed in order to study the stability in the same way. Therefore, the region of small velocity defined as $|v_{rel}| < \epsilon$ will be considered as the stick mode while we will consider that we have a slip mode when the

relative velocity lies outside of this narrow band. The map P_{trans} is well defined if stick-slip transitions occur for all transient and steady state motions. This condition is satisfied for our system with the parameter values that we use.

To calculate one-parameter bifurcation diagrams, a brute-force method has been used. For each value of ω an initial condition is considered. Then, the system is simulated during a certain time (1200 periods, i.e. $1200 \cdot \frac{2 \cdot \pi}{\omega}$) and we plot the transition points from stick to slip for the last 1000 periods. The drawback of this method is that it only shows stable solutions. For calculating the unstable solutions we will use the map described before.

Simulations of two-parameter bifurcation diagrams have been obtained using numerical continuation techniques based on shooting. For the case of the degenerate switching-sliding bifurcation algorithms, developed for sliding bifurcations [54] have been used. The smooth cusp codimension-two bifurcation has been detected and continued using smooth continuation methods [130].

Finally, in order to get a complete global analysis of the system we need to give the entire phase portrait, with attractors, their basins of attractions, invariant manifolds, unstable limit set, etc. By means of a standard *cell-to-cell mapping* algorithm we simulate domains of attraction (DOAs) of coexisting solutions. The method of cell mapping for the study of dynamical systems was developed by Hsu [84], who also provided a detailed mathematical foundation for the technique. In this method the domain of interest is divided into a number of equally sized squares. The center point of each square is mapped forward in time one period and the location of the trajectory at this point is recorded. This is done for each square and finally all data is post-processed to build the complete picture, displaying where initial conditions will end up as $t \to \infty$. Obviously, the smaller each cell is, the more refined the final picture will be.

4.6 Numerical analysis of the system

In this section we will show different dynamical scenarios related with the four distinct cases of sliding bifurcations. The first scenario is depicted in Fig. 4.5 (a). This picture shows a bifurcation diagram for $A = 0.5$ and $\omega \in [2.84, 2.94]$.

As can be observed, different behaviors are exhibited in this range and DIBs are found, such as adding-sliding and grazing-sliding bifurcations. Looking at the bifurcation diagram a stable period-one orbit is initially

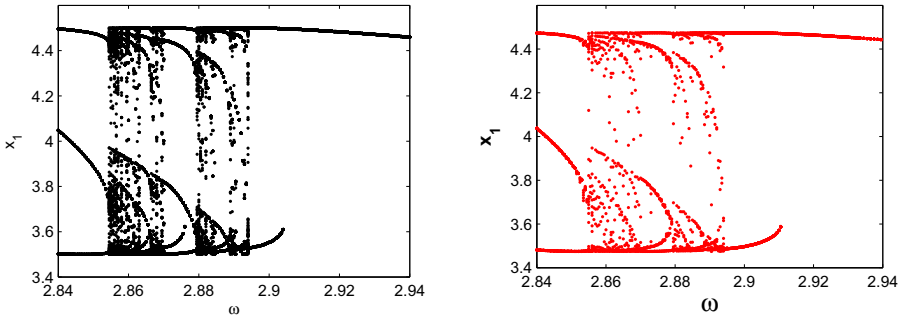

(a) (b)

Figure 4.5: Bifurcation diagram: (a) Event-driven method (b) Smoothing method

found for $\omega = 2.94$. However an unstable period-one solution is also found as can be seen in Fig. 4.6(a). There are two points lying on the bisection line: one orbit ($\phi \approx 0.5$) is stable because the slope of the map P_{trans} at this point is less than 1; the other orbit ($\phi \approx 3.5$) is unstable because the slope at this point is larger than 1. Decreasing the value of ω, these solutions exist until the value $\omega = 2.904315905$. Then, an adding-sliding bifurcation occurs, for which the system presents a stable periodic orbit with two transition points from stick to slip. Fig. 4.7 shows how the periodic orbit hits tangentially the boundary of the sliding region and hence, further variation of the parameter splits the initially unique stick phase into two stick phases separated by a slip phase. In this figure the stick motion is represented by the black line and $\partial\Sigma^{-}$is the blue line. Fig. 4.7(c)-(d) show how the velocity time-history is affected by the bifurcation. After the bifurcation, the stable periodic orbit is characterised by two stick-slip transition points whereas the unstable periodic orbit remains with the same shape. Fig. 4.6 (b) shows the second iterate of the map P_{trans} for $\omega = 2.9$ in order to illustrate the new scenario.

To carry out the analytical investigation of the bifurcation point under consideration, we will check that the set of analytical conditions (see [51]) are satisfied at the bifurcation point under investigation. The bifurcation occurs when $\omega = 2.904315905$ and the bifurcation point is $(x_1^*,\, x_2^*,\, x_3^*) = (4 + 0.5\cos(x_3^*),\, 1,\, x_3^*) = (3.63744370156881,\, 1,\, 3.9011910917405)$. There-

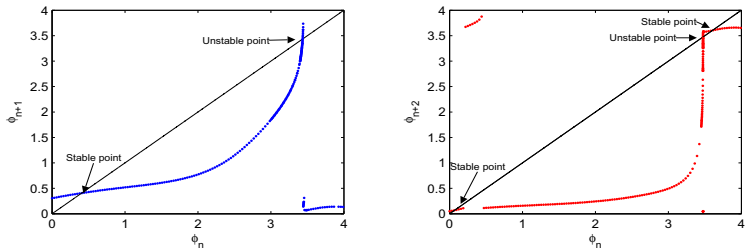

(a) (b)

Figure 4.6: (a) Map of the phase angle ϕ at the stick-slip transition ($\omega = 2.94$). (b) Second iterate of the map at the stick-slip transition ($\omega = 2.9$).

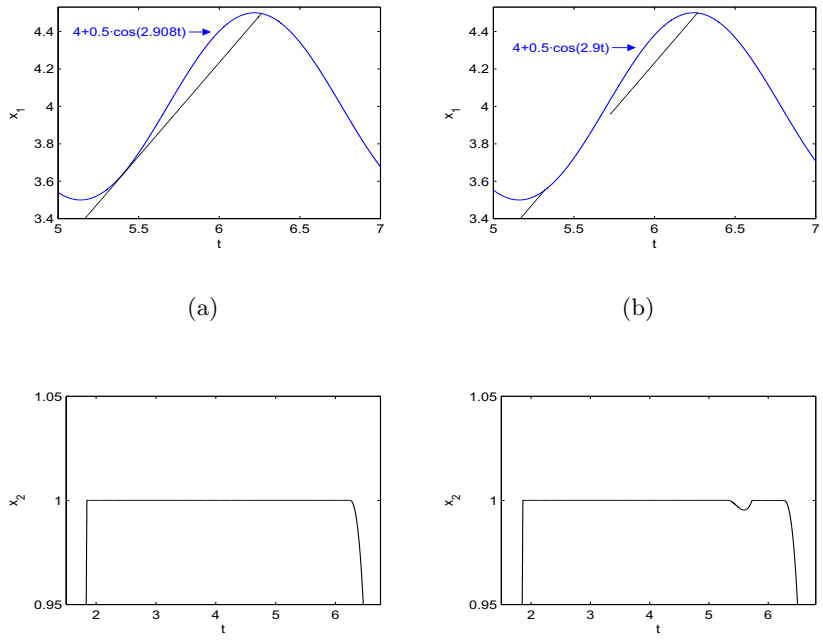

(a) (b)

(c) (d)

Figure 4.7: (a) Map of the phase angle ϕ at the stick-slip transition ($\omega = 2.94$). (b) Second iterate of the map at the stick-slip transition ($\omega = 2.9$).

fore, we calculate the following set of analytical conditions:

1. h(x^*)=0,
2. s(x^*)=-1,
3. $\langle \nabla h, F_{1x} F_1 \rangle|_{x^*}$=$1 + 0.5 \cdot 2.904315905 \cdot \sin(3.9011910917405) = 0$,
4. $\langle \nabla h, F_{1x}^2 F_1 \rangle|_{x^*}$=$3 \cdot 1.42 \cdot (1 + 0.5 \cdot 2.904315905 \cdot sin(3.9011910917405)) = 0$,
5. $\langle \nabla h, F_{1x} F_{1xx} F_1 F_1 \rangle|_{x^*} + \langle \nabla h, F_{1x}^3 F_1 \rangle|_{x^*}$=$3 \cdot 1.42 \cdot 0.5 \cdot \omega^* \cdot \cos(3.9011910917405) < 0$.

Thus, we have checked the analytical conditions and observed a degenerate adding-sliding bifurcation (see [51] for further details).

Decreasing the parameter value ω to 2.8942, we found a grazing-sliding at this point. As can be seen in Fig. 4.8 both stable and unstable periodic orbit disappear when a further variation of the bifurcation parameter is carried out. This happens because a section of trajectory grazes the boundary of the sliding region (see Fig. 4.8 (c)-(d)).

The bifurcation point is $(x_1^*, x_2^*, x_3^*) = (4 + 0.5cos(x_3^*), 1, x_3^*) = (4.49954991480195, 1, 0.04243360648476)$ and the analytical conditions at the bifurcation point are:

1. h(x^*)=0,
2. s(x^*)=-1,
3. $\langle \nabla h, F_{1x} F_1 \rangle|_{x^*}$=$1 + 0.5 \cdot 2.8942 \cdot sin(0.04243360648476) > 0$.

Thus, at the aforementioned value of x^*, the system satisfies all three conditions and it is therefore proven that the bifurcation event is due to a grazing-sliding bifurcation. We can observe the sudden appearance of a chaotic attractor when ω is decreased, which can be explained analytically using the theory of border-collisions [120]. In order to classify this bifurcation a Poincaré map is needed and a discontinuity map must be obtained. This map has a piecewise linear functional form and therefore, the grazing-sliding bifurcation under investigation corresponds to a so-called border-collision bifurcation. Then, counting the number of real eigenvalues of the piece-wise linear map on both sides of the discontinuity boundary we can classify such bifurcation using the classification scheme proposed in [**?**].

Figure 4.5 (b) shows the bifurcation diagram in the same range for ω but we have used a smoothing method. As explained in section 4.5 a

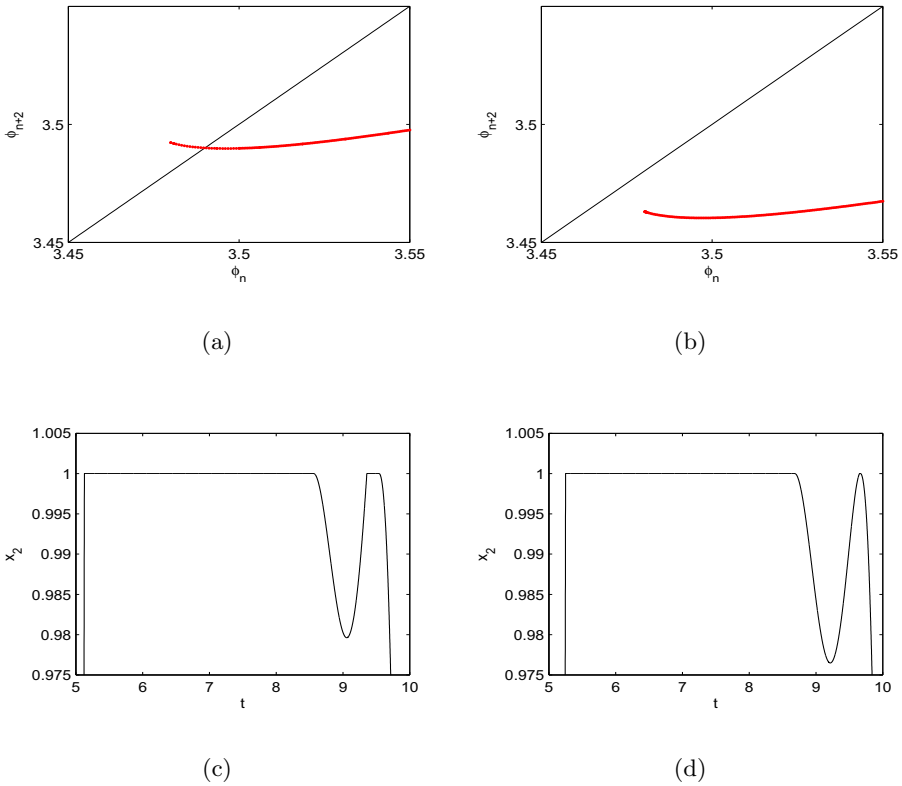

Figure 4.8: (a) Second iterate of the map at the stick-slip transition ($\omega = 2.895$) (b) Second iterate of the map at the stick-slip transition ($\omega = 2.893$).

stick mode does not exist and in order to obtain a similar map we consider that the stick mode is defined by the relative velocity lying inside of a narrow band given by $|v_{rel}| < \epsilon$. The two pictures are very similar but nevertheless there are some differences. For example, the bifurcation event due to the adding-sliding is found at a different value of ω. However, we can conclude that the smoothing approach gives us the same behaviour as using an event-driven method but more time for the simulation is needed.

Now we will show the other two sliding bifurcations considering $A = 5$. In Fig. 4.9 we depict a periodic orbit without a sticking mode for $\omega = 1.6$. This orbit continues until $\omega = 1.65768$ and then a crossing-sliding bifurcation occurs. The periodic orbit intersects the boundary of the sliding region

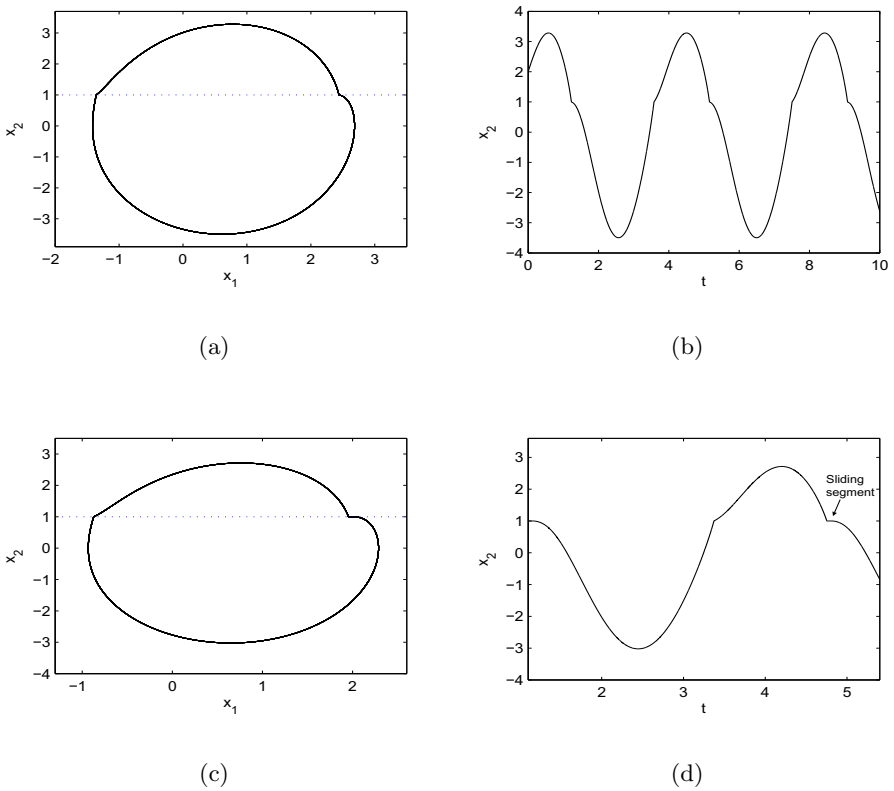

(a) (b)

(c) (d)

Figure 4.9: (a) Periodic orbit ($\omega = 1.6$) (b) Time evolution ($\omega = 1.6$) (c) Periodic orbit ($\omega = 1.72$) (d) Time evolution $\omega = 1.72$).

and further variations of ω give a periodic orbit with a sliding segment (see Fig. 4.9).

Analytically we can check the conditions for a crossing-sliding bifurcation. The bifurcation point is $(x_1^*,\ x_2^*,\ x_3^*) = (4 + 5cos(x_3^*),\ 1,\ x_3^*) = (2.19098042496318,\ 1,\ 4.34218680843852)$, and we have that the following three analytical conditions

1. h(x^*)=0,
2. s(x^*)=-1,
3. $\langle \nabla h, F_{1x} F_1 \rangle|_{x^*}$=$1 + 5 \cdot 1.65768 \cdot sin(4.34218680843852) > 0$.

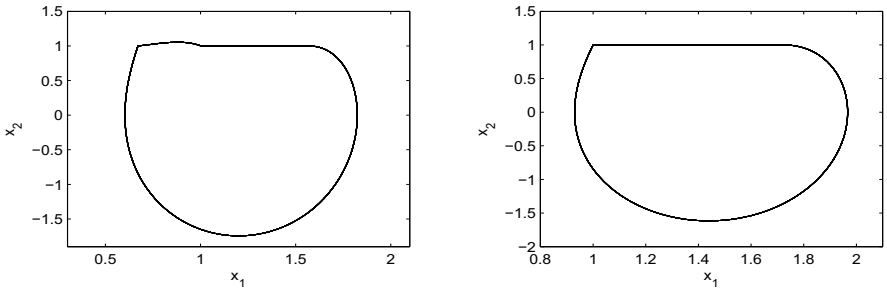

(a) (b)

Figure 4.10: (a) Periodic orbit ($\omega = 2.5$) (b) Periodic orbit ($\omega = 2.8$).

are satisfied.

Finally we present a switching-sliding bifurcation at $\omega = 2.7992$. In this case the periodic orbit hits the sliding boundary $\partial\Sigma^+$ at the bifurcation point. For $\omega = 2.5$ the periodic orbit goes from negative relative velocity to positive and from this to the sliding region. Past the bifurcation event the periodic orbit is completely contained in the subspace of negative relative velocity and the sliding region (see Fig. 4.10).

The bifurcation point is $(x_1^*, x_2^*, x_3^*) = (-4+5cos(x_3^*), 1, x_3^*) = (0.99907076368474, 1, 0.01927967945125)$, and it must verify the following analytical conditions:

1. h(x^*)=0,

2. s(x^*)=1,

3. $\langle \nabla h, F_{2x} F_2 \rangle|_{x^*} = 1 + 5 \cdot 2.7991 \cdot sin(0.01927967945125) > 0.$

Thus, at the aforementioned value of x^*, the system satisfies all three conditions and it is therefore proven that the bifurcation event is due to a switching-sliding bifurcation. Notice that the analytical conditions (2) and (3) do not correspond with (4.25) and (4.27) because we have considered the sliding boundary $\partial\Sigma^+$ instead $\partial\Sigma^-$. Using condition (4.27) with F_2 changes the sign, which must be positive at the switching-sliding bifurcation point, as it is.

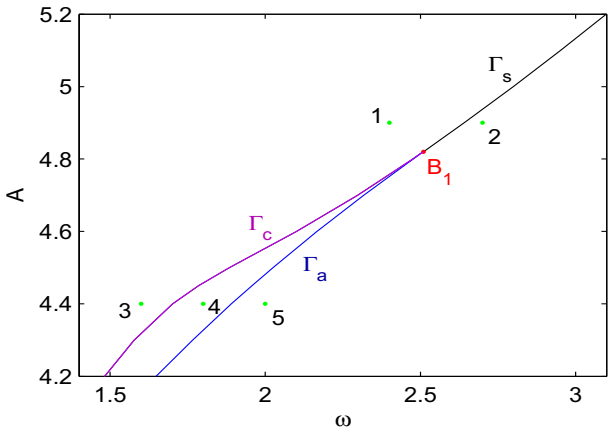

Figure 4.11: Two parameter bifurcation diagram around the codimension-two points.

4.7 Two-parameter Nonsmooth Bifurcation

In [92] a first classification approach for codimension-two DIB is proposed. Basically, codimension-two DIB for limit cycles can be put into one of the following three types: degenerate points, C-bifurcations of degenerate cycles and simultaneous occurrence of two bifurcations. In this section we will show a codimension-two C-bifurcation due to a degenerate sliding bifurcation.

As we have previously seen a switching-sliding bifurcation occurs for $A = 5$ and $\omega = 2.7992$. Varying A we found a bifurcation curve including the aforementioned bifurcation point that we will term Γ_s (see Fig. 4.11). Following the periodic orbits along Γ_s the analytical conditions for the switching-sliding bifurcation scenario presented in section 4.6 are verified for $A > 4.82$. However, considering $A = 4.82$ the condition $\langle \nabla h, F_{2x} F_2 \rangle|_{x^*} > 0$ is violated because it becomes zero. The condition $\langle \nabla h, (F_{2x})^2 F_2 \rangle|_{x^*} > 0$ is satisfied and therefore the set of analytical conditions determine a degenerate codimension-two switching-sliding bifurcation.

The switching-sliding bifurcation curve branches out from the point B_1 and two new curves of codimension one are generated. These are crossing-sliding and adding-sliding bifurcation curves and we will denote them by Γ_c and Γ_a respectively. In Fig. 4.11 the three curves are depicted using

numerical continuation techniques. We have plotted different points around the codimension-two point B_1 in order to explain the behaviour in each part of the two parameter bifurcation diagram. Periocidity and stability of such periodic orbit remain unchanged and the only effect is the creation of additional segments of the orbit due to interactions with the sliding boundaries.

Points 1 and 2 represent the orbits before and after crossing the bifurcation curve Γ_s for $(\omega, A) = (2.4, 4.9)$ and $(\omega, A) = (2.7, 4.9)$ respectively. These orbits are depicted in Fig. 4.12 (a)-(b) and correspond to the typical switching-sliding bifurcation scenario that we have presented in Section 4.6.

Fig. 4.12 (c)-(e) depict the orbits in points 3, 4 and 5. The periodic motion of Point 3, $(\omega, A) = (1.6, 4.4)$, has two slipping phases and a sticking phase. An increase in ω to Point 4, $(\omega, A) = (1.8, 4.4)$, crosses the bifurcation curve Γ_c where a crossing-sliding bifurcation occurs. The periodic motion of Point 4 has 2 slip phases alternated with two stick phases. A new increase in ω brings about an adding-sliding bifurcation, crossing the curve Γ_a. The orbit of Point 5 is completely contained in the region defined by $|v_{rel}| \leq 0$ (see point 5, $(\omega, A) = (2, 4.4)$).

4.8 Cusp bifurcation and coexistence of attractors

In this section we present a smooth cusp codimension-two bifurcation. As can be seen in Fig. 4.13, from the codimension-two point B_2, a cusp point, two branches of fold bifurcation merge tangentially (which we shall denote by Γ_{f1} and Γ_{f2}). The resulting wedge divides the parameter plane into two regions. In region **1**, inside the wedge, there are three solutions (see Fig. 4.14), two stable and one unstable, while in the other region, outside the wedge, there is a single solution, which is stable.

Varying ω and crossing either Γ_{f1} or Γ_{f2} away from the cusp point we find a nondegenerate fold bifurcation. However, if we approach the cusp point from inside region **1**, all three solutions merge together into a *triple* root solution, see Fig. 4.14. Figures 4.14 (c)-(d) show the fold scenarios of each curve Γ_{f1} and Γ_{f2}.

By means of the simple cell-to-cell mapping method, a domain of attraction diagram is depicted in Fig. 4.15 for $(A, \omega) = (3.6, 1.067)$. We have divided the phase space region into 500×500 cells to plot the scenario in this point which is inside the wedge of the parameter space and therefore, three fixed points are found. The three orbits are period one and have been depicted in Fig. 4.15 (a). Black points represent the stable solutions and

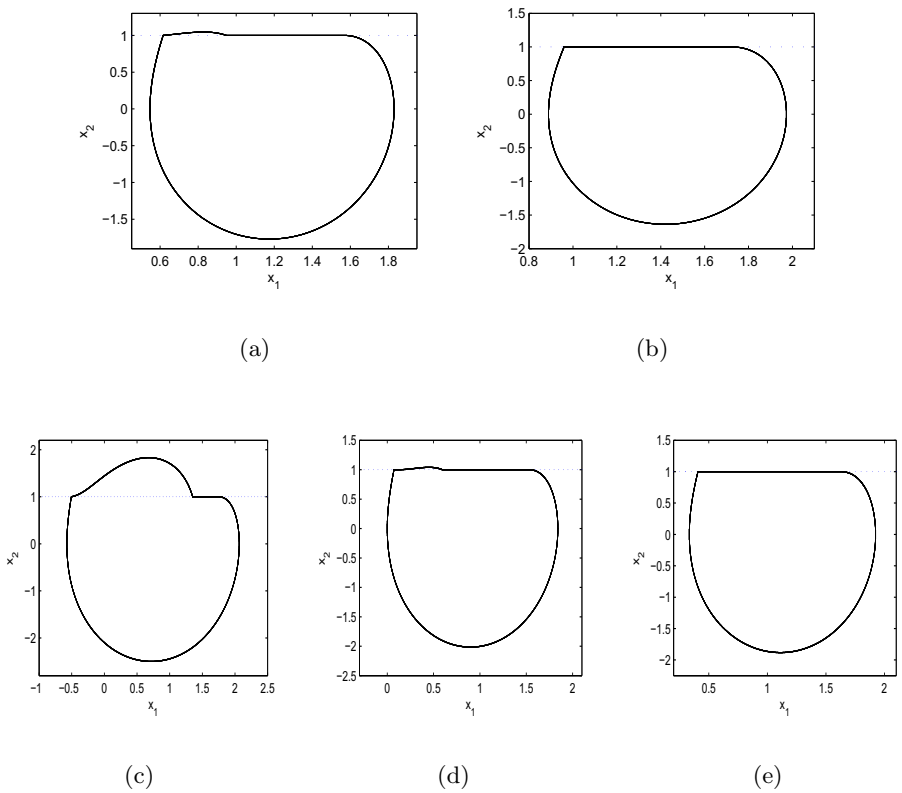

Figure 4.12: Phase space corresponding to: (a) Point 1, (b) Point 2, (c) Point 3, (d) Point 4, (e) Point 5.

the green point is the unstable one.

Figure 4.15 (a) shows the different basins of attraction for the two stable solutions of Fig. 4.16. The yellow region yields the solution of Fig. 4.16 (a), and initial conditions from the dark red lead to the solution of Fig. 4.16 (b). The basins of attraction are separated by the stable invariant manifold of the saddle-node solution. As can be seen such invariant manifold seems continuous but does not appear to be continuously differentiable because of the appearance of corners. In Fig. 4.15 (b) we have plotted the number of iterates (transient times) of each cell before landing on one of the stable cycles. In this picture we can see the global time behaviour of the phase portrait, *i.e.*, the time needed for each initial condition to

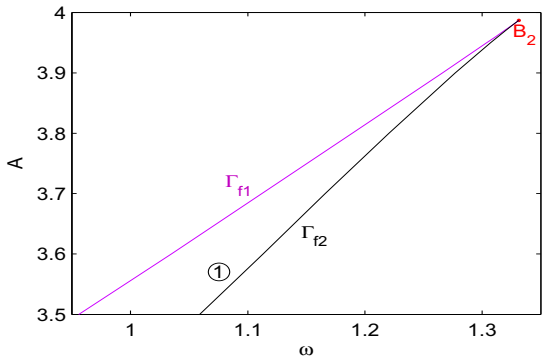

Figure 4.13: Two-parameter bifurcation diagram showing the cusp bifurcation.

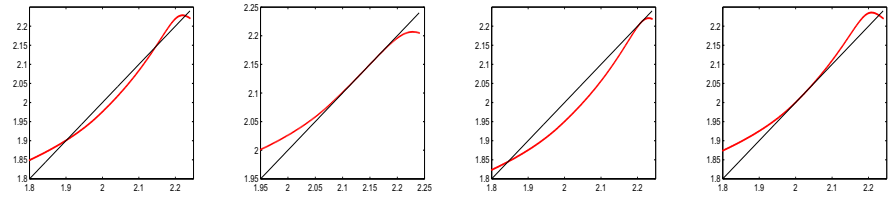

(a) (b) (c) (d)

Figure 4.14: Different scenarios of the map P^2_{trans}: (a) Region **1** (b) Cusp point (c) Curve Γ_{f1} (d) Curve Γ_{f2}.

reach its attractor. For example, we can observe that the points near to the mentioned invariant manifold take more than 60 iterations (dark red) to stabilize while the periodic orbits have zero transient time (dark blue).

4.9 Conclusions

In this chapter we have investigated a dry friction oscillator using a measured friction characteristic introduced in [125]. This system is affected by sliding bifurcations and an example of each of the four possible cases (crossing-sliding, grazing-sliding, switching-sliding and adding-sliding) has

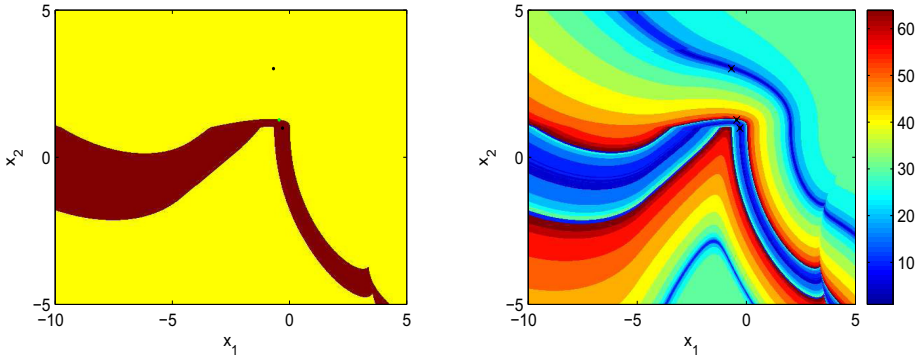

(a) (b)

Figure 4.15: Domain of attraction using a cell-to-cell mapping method for $(A, \omega) = (3.6, 1.067)$ (a) Basins of attraction (b) Transient time.

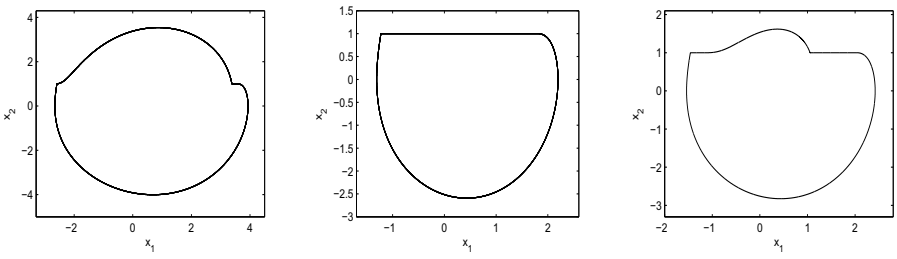

(a) (b) (c)

Figure 4.16: Coexistence of periodic solutions for $(A, \omega) = (3.6, 1.067)$ with initial conditions (a) $(x_{10}, x_{20}) = (-0.685, 3.01)$ (b) $(x_{10}, x_{20}) = (-0.295, 0.99)$ (c) $(x_{10}, x_{20}) = (-0.445, 1.27)$.

been identified.

Codimension-two bifurcations have been also calculated. Firstly, a degenerate switching-sliding bifurcation has been shown. Furthermore, a smooth cusp codimension-two bifurcation has also been presented. Coexistence of two stable solutions and an unstable solution in the parameter region have

been depicted in a domain of attraction diagram. The stable invariant manifold of the saddle-node point splits the basins of attraction of each stable solution. This invariant manifold is continuous but not differentiable, *i.e.* a nonsmooth invariant manifold. The study of this kind of invariant manifolds, that are typically found in nonsmooth systems, is a subject of further research.